

Unraveling the origin of antiferromagnetic coupling at YIG/permalloy interface

Jiangchao Qian,¹ Yi Li,² Zhihao Jiang,¹ Robert Busch,¹ Hsu-Chih Ni,¹ Tzu-Hsiang Lo,¹ Axel Hoffmann,¹ Andre Schleife,¹ and Jian-Min Zuo¹

¹Materials Research Laboratory and Department of Materials Science and Engineering,
University of Illinois at Urbana-Champaign, Urbana, Illinois 61801, USA

²Materials Science Division, Argonne National Laboratory, Argonne, IL 60439, USA

(Dated: February 23, 2024)

We investigate the structural and electronic origin of antiferromagnetic coupling in the Yttrium iron garnet (YIG) and permalloy (Py) bilayer system at the atomic level. Ferromagnetic Resonance (FMR) reveal unique hybrid modes in samples prepared with surface ion milling, indicative of antiferromagnetic exchange coupling at the YIG/Py interface. Using scanning transmission electron microscopy (STEM), we highlight significant interfacial differences introduced by ion-milling. The observations suggests that the antiferromagnetic coupling in YIG/Py bilayers is predominantly driven by an oxygen-mediated super-exchange coupling mechanism on the tetrahedral Fe terminated YIG surface, which is supported by density functional theory calculations. This research provides critical insight into the fundamental mechanisms governing the efficiency of coupling in magnetic bilayers and underscores the pivotal role of oxide surface termination in modulating magnetic interfacial dynamics.

Yttrium iron garnet ($\text{Y}_3\text{Fe}_5\text{O}_{12}$) is well-known for its low magnetic damping [1–3], making it the material of choice for efficient spin interactions in magnonics [4–7], spin transport [8], cavity spintronics [9–12], and quantum information science [13, 14]. Considerable attention has been directed toward building YIG-based thin film heterostructures for spin-based information processing by taking advantage of interfacial spin interactions. One example is the YIG/Pt bilayers, with experimental observations of spin pumping [15], nonlocal spin injection [8], and spin Hall magnetoresistance [16], where the interlayer exchange coupling has significantly enhanced the spin transmission across the YIG-Pt interface.

Recently, another YIG heterostructure with a ferromagnetic (FM) layer, i.e. YIG/FM bilayer, has aroused increasing interests owing to its potential in hybrid magnonics from the interlayer magnon-magnon coupling [17–20]. The ferromagnetic resonance mode in the FM layer can form strong coupling with the perpendicular standing spin wave modes in YIG due to the interfacial exchange interaction, leading to new physical phenomena such as coherent spin pumping [20], magnetically induced transparency [21], and efficient excitations of short-wavelength spin waves [22]. However, the physical mechanisms underlying the interfacial exchange coupling, crucial for coupling spin excitations between the two magnetic systems, remain not fully understood. Particularly, recent works have revealed pronounced antiferromagnetic coupling across YIG/CoFeB, YIG/Co and YIG/Py interfaces, where the origin of antiferromagnetic coupling between YIG and FM layers has been a topic of considerable debate. Separately, Luqiao et al. [23, 24], and Stefan et al. [25] have posited theories of direct exchange coupling, while the possibility of super-exchange coupling also remains. This debate is further confounded by the absence of conclusive experimental evidence at the atomic scale and the inherent challenges in characterizing metal-oxide interfaces, where factors like surface

termination and interface chemistry are crucial. Previous studies, reported either ferromagnetic coupling or antiferromagnetic coupling in different prepared YIG/FM bilayers. These findings hint at the significant role of interfacial structure in determining bilayer coupling mechanisms, yet this aspect remains insufficiently explored. Here we elucidate the interface structure between YIG and Py and their magnetic coupling. By integrating Ferromagnetic Resonance (FMR) with advanced STEM and spectrscopy, and DFT calculations, our study reveals the significant role of surface treatments using ion-milling in enhancing antiferromagnetic coupling through promoting the oxygen mediated super-exchange coupling mechanisms at the YIG/Py interface.

In line with the preparation of YIG/Py bilayer in our prior work [20], we first deposited YIG (100 nm) onto two (111)-oriented $\text{Gd}_3\text{Ga}_5\text{O}_{12}$ substrates by magnetron sputtering. Then the amorphous YIG films was annealed in air at 850 °C for 3 hours, and slowly cooled down to room temperature by 0.5 °C/min, yielding epitaxial YIG films with light yellow color. To study the formation of antiferromagnetic interfacial exchange coupling, we slightly ion milled one YIG film in the sputtering chamber under Ar environment by applying an RF bias voltage through the substrate holder, where the holder acts as an effective sputtering gun and trigger Ar^+ ion bombarding of the substrate surface. The milling rate was 3 nm/mins and the milling process lasted for 1 min 30 s. A Py (10 nm) thin film was subsequently sputtering on the milled YIG film without breaking the vacuum, ensuring efficient interfacial exchange coupling. A control YIG/Py bilayer sample was also prepared without ion milling the YIG surface. Figure 1a shows the cross-sectional film structure. The quality of the bilayers were checked using X-Ray Diffraction. Clear (444) peaks of YIG and GGG were measured along with Laue oscillations, indicating that both samples possess high film quality and maintain epitaxial relationships (Suppl.

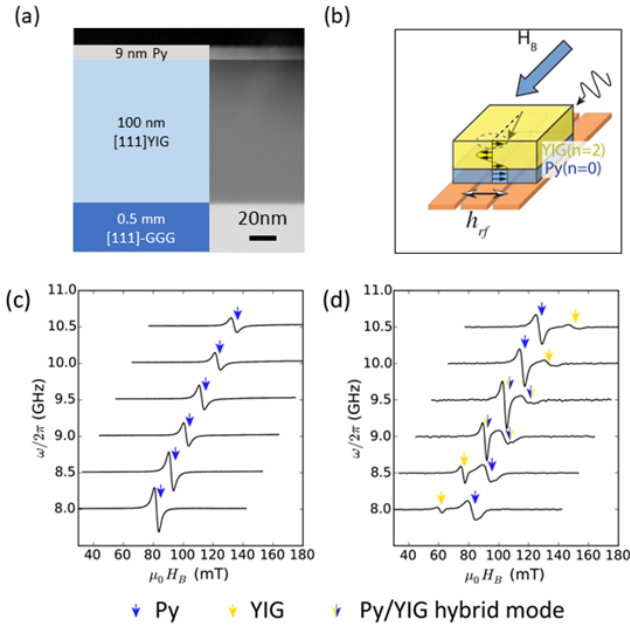


FIG. 1. The YIG/Py bilayer structure and FMR characterization. (a) STEM image together with the designed bilayer structure. (b) A illustration of the FMR setup: The coplanar waveguide is located underneath the YIG/Py bilayer thin films. (c)-(d): FMR induced magnetization excitations in YIG/Py bilayer samples on top of the coplanar waveguide. The Line shapes of (c) without ion-milling and (d) with ion-milling samples for the first three resonance modes of YIG and the uniform mode of Py.

FIG. 1). The two samples we prepared will be named subsequently as IM for with ion milling and WoIM for without ion milling.

We first conducted a FMR measurement on the two samples we prepared with and without ion milling. Figure 1b details this experimental arrangement using the same setup with the coplanar waveguide beneath the YIG/Py bilayer as in our previous work [20]. The FMR results are depicted in FIG. 1c and 1d, showing FMR-induced magnetization excitations in the YIG/Py bilayer samples. Notably, two hybrid modes are present in the ion-milled samples, but absent in those without ion-milling. As illustrated in FIG. 1d, these observed hybrid modes in the YIG/Py bilayer system's spin pumping experiment signify antiferromagnetic exchange coupling at the interface. The broader linewidth mode, exhibiting a higher resonance field than the narrower linewidth mode, acts as a key indicator of this antiferromagnetic coupling. This finding is discussed in detail in our previous work [20].

To investigate the structural origin of the magnetic differences between samples with and without ion-milling, we performed cross-sectional STEM of the YIG/Py bilayer films using a high-angle annular dark-field detector (HAADF) for Z-contrast (details in Suppl. Notes). Figure 2a shows the STEM-HAADF images of the two

samples, providing an atomic-scale inspection of their interfacial structural differences. The YIG surface termination in the IM sample, as revealed in FIG. 2a, comprises a plane of visible Fe and Y atoms, and invisible O atoms, leading to an interface layer that sharply connects to the polycrystalline Py. In contrast, the interface in the WoIM sample exhibits roughness and features an amorphous layer approximately 0.7 nm in width (Fig. 2b). The direct adjacency of the termination plane to the Py layer in the IM sample eliminates the observed gap in the WoIM sample. This distinction in interfacial structure between the two samples is further substantiated by the normalized intensity line profiles depicted in FIG. 2c. The YIG surface termination in the IM sample is further examined in FIG. 2d, with line profiles marked in FIG. 2a. These profiles demonstrate that the termination plane ends with a combination of Y and Fe containing atomic columns, with Py atoms directly adjoining the crystalline garnet structure in the IM sample.

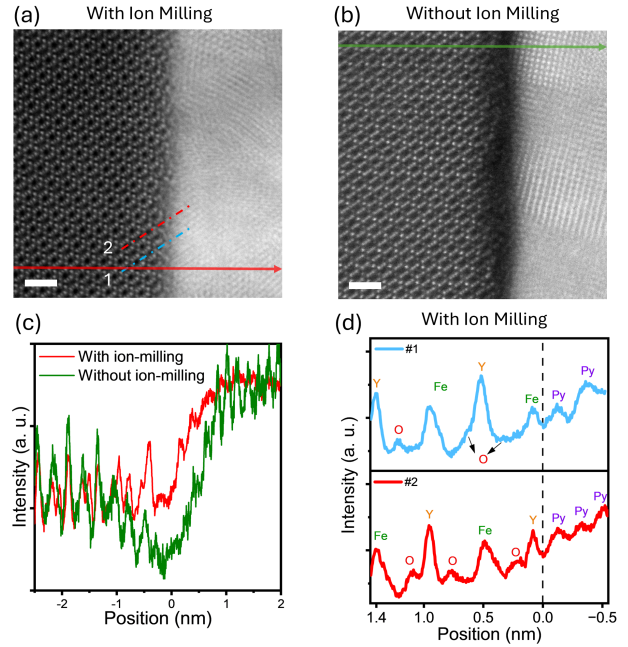


FIG. 2. Interfacial structure as seen by atomic-resolution STEM-HAADF along the YIG [110] zone axis. STEM-HAADF images for the with ion-milling (a) and without ion-milling (b) samples. The scar bars are both 0.5 nm. (c) The corresponding horizontal line profiles of HAADF image shows the different YIG/Py interfaces in (a) and (b). (d) The line profiles of normalized intensity across the dashed lines in (a), showing the termination of Y and Fe, with Py atoms adjacent to YIG.

From our STEM-HAADF observations, the garnet structure appears consistent up to the interface, suggesting a minimal structural modification. Electron energy loss spectroscopy (EELS) analysis was performed in the STEM mode to further examine the chemical sharpness of the YIG/Py interface in the IM sample. Figures 3a,b display the oxygen K-edge fine structure, alongside

a HAADF survey image (FIG. 3c) with a sampling resolution of 0.5 nm. This combination provides insights into both the oxygen content and the nature of its chemical bonding. The oxygen K-edge fine features are observed up to the interface. A drop in the K-edge intensity is observed near within the distance of 1 nm to the interface, which can be attributed to the electron probe spreading effect [26]. In addition to the pre-peak for oxygen, the fine features in the range of 535 eV to 540 eV also exhibit changes near the interfaces, indicative of slightly altered yttrium-oxygen (Y-O) bonding. Figures 3d,e showcase the EELS fine structures for the Fe L₃-edge, coupled with a HAADF survey image. The lower layer consists of Fe⁰ from Py, while the upper layer contains Fe³⁺ from YIG. The evolution of the oxygen K-edge and Fe L₃ edge are further highlighted in FIG. 3b,e, which plot the hyperspectral EELS data versus the STEM probe position. At the interface, the Fe L₃ EELS signal is approximately a composite of Fe⁰ and Fe³⁺, while oxygen is detected up to the interface. The presence of oxygen at the interface and slightly beyond and its sharper transition than the L₃ edge of Fe suggests an oxygen terminated YIG surface. The coexistence of Fe⁰ and Fe³⁺ in the interfacial transition region suggests a small amount of interfacial defects, possibly Fe interstitial atoms inside a rather open YIG structure.

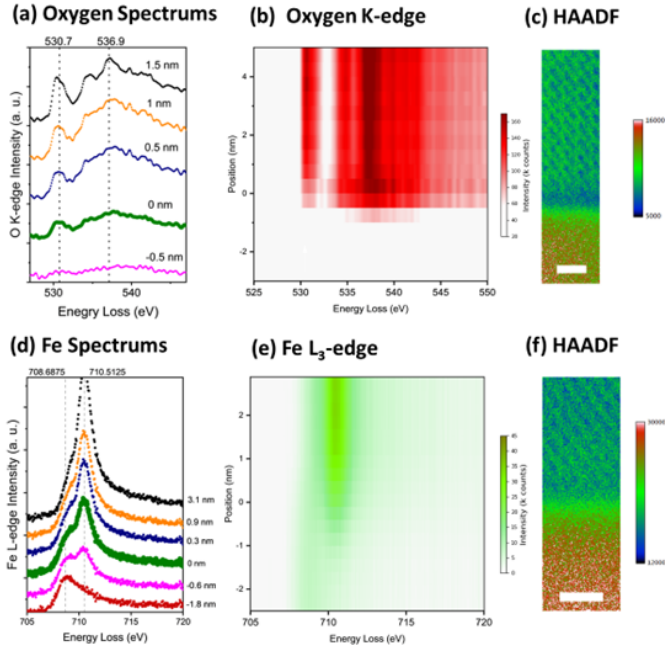


FIG. 3. With ion-milling sample: The mono EELS fine structure spectrums for (a) oxygen K-edge; and (d) iron L₃-edge, where the position markers are corresponding to the position in right side HAADF image (c) and (f), respectively. Integrated 1D spectrum across the interface shows the peak evolution for oxygen K-edge (b) and (e) Iron L₃-edge. The scar bars are both 1 nm in (c) and (f).

To integrate our experimental results with theoretical

insights, we employed Density Functional Theory (DFT) calculations to simulate the YIG/Py interfacial configurations. The interface structural model we proposed are depicted in FIG. 4a,b. The YIG (111) surface is terminated with yttrium coordinated by 8 oxygen ions and tetrahedral coordinated Fe, respectively. The superposition of the YIG structural motifs on the magnified atomic resolution image from FIG. 2a shows the good agreement between the model and the observed interfacial atomic arrangements. The Py atoms, which are not individually resolved in FIG. 4a, appear slightly disordered due to interactions with the YIG surface. For simplicity, we have assumed a two perfect layer of Py atoms parallel to the YIG surface in our model. The whole supercell consists of 294 atoms. Figure 4c showcases the calculated density of states for Fe and oxygen (see Suppl. notes for details).

Two potential magnetic arrangements can exist at the YIG/Py interface: antiferromagnetic (AFM), where bulk YIG and Py have opposite magnetic moments, and ferromagnetic with same magnetic moments. Using the structure model in FIG. 4b, we performed spin-polarized DFT calculation with different Fe and Ni arrangements in Py. The results indicate that the AFM arrangement is energetically more favorable than FM arrangement with an average energy difference of 0.62 eV per simulation cell. On the contrary, when we placed the Py atoms on the opposite side of the YIG slab, we found dominate FM coupling at this interface. Within the YIG, octahedral Fe and tetrahedral Fe are antiferromagnetic coupled, while the tetrahedral Fe provides the dominant spin. In the AFM arrangement, the spins of tetrahedral Fe are also antiferromagnetic coupled with Py atom. The DFT simulation results thus supports our experimental observation of AFM in the ion-milled sample where the tetrahedral Fe ions interact with Py atoms with the mediation of oxygen ions as highlighted by circles in Fig. 4b. The surface on the YIG without the ion-milling in comparison are rough with a mixture of surface terminations in addition to the amorphous-like layer that breaks the AFM coupling between bulk YIG and Py.

We further note that ion-milling not only sharpens the interface between YIG and Py but also activates their bonding, with minimal impact from oxygen loss. This process may also lead to distortions in the garnet structure, which in turn could enhance the antiferromagnetic super-exchange coupling due to reduced crystal-field splitting energy. While the Goodenough-Kanamori-Anderson (GKA) rules typically govern antiferromagnetic (AF) coupling in Fe-O-Fe bondings, they are less predictive when the structure becomes distorted. However, the introduction of interstitial atoms, particularly Fe⁰, is expected to maintain the AF trend. Given the co-existence of Fe⁰, Fe³⁺, and oxygen at the YIG/Py interface, we propose that oxygen-mediated super-exchange coupling could be the predominant mechanism for the antiferromagnetic interaction between Py and YIG, conceptualized as $\langle Fe^0 | Up \rangle - - O - - \langle Fe^{3+} | Down \rangle$. The substitution of Ni⁰ for Fe⁰ likely does not alter the di-

rection of the magnetic moments. This insight is crucial in our discussion, as it suggests that the antiferromagnetic coupling between Py and YIG is predominantly driven by oxygen-mediated super-exchange coupling, a key finding of this study.

In summary our study explored the magnetic, structural, and electronic properties of YIG/Py bilayer samples, comparing those with and without ion-milling. FMR measurements revealed unique hybrid modes in ion-milled samples, indicative of antiferromagnetic exchange coupling at the YIG/Py interface. DFT calculations integrated with experimental STEM/EELS findings, showing the critical role of tetrahedral Fe terminated YIG surface in providing an energetically preferable antiferromagnetic arrangement at the YIG/Py interface. Altogether, these findings, coupled with the observed oxygen-mediated super-exchange coupling mechanism, suggest that the antiferromagnetic coupling between Py and YIG is predominantly driven by this mechanism.

Acknowledgement. The work was supported by the U.S. DOE, Office of Science, Basic Energy Sciences, Materials Sciences and Engineering Division, with all parts of the manuscript preparation supported under contract No. DE-SC0022060.

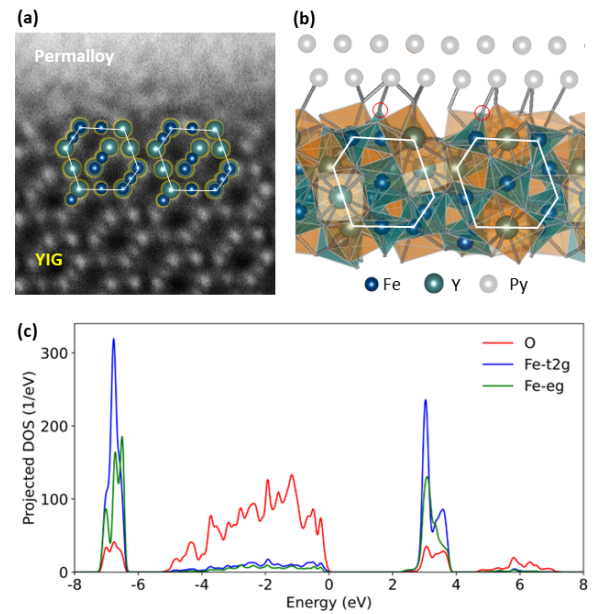


FIG. 4. (a) Zoomed-in HAADF image in FIG. 2a showing the overlap with YIG motif structures at terminations. (b) Relaxed YIG/Py slab model via Density Functional Theory (DFT) simulation. Highlighted white hexagons represent YIG motifs. Both (a) and (b) are illustrated at [110] projection. (c) Density of States calculated via DFT for pristine YIG.

[1] Y. Sun, H. Chang, M. Kabatek, Y.-Y. Song, Z. Wang, M. Jantz, W. Schneider, M. Wu, E. Montoya, B. Kardasz, B. Heinrich, S. G. E. te Velthuis, H. Schultheiss, and A. Hoffmann, Damping in yttrium iron garnet nanoscale films capped by platinum, *Phys. Rev. Lett.* **111**, 106601 (2013).

[2] M. B. Jungfleisch, W. Zhang, W. Jiang, H. Chang, J. Sklenar, S. M. Wu, J. E. Pearson, A. Bhattacharya, J. B. Ketterson, M. Wu, and A. Hoffmann, Spin waves in micro-structured yttrium iron garnet nanometer-thick films, *Journal of Applied Physics* **117**, 17D128 (2015), https://pubs.aip.org/aip/jap/article-pdf/10.1063/1.4916027/13619252/17d128_1_online.pdf.

[3] C. Hauser, T. Richter, N. Homonay, C. Eisenschmidt, M. Qaid, H. Deniz, D. Hesse, M. Sawicki, S. G. Ebbinghaus, and G. Schmidt, Yttrium iron garnet thin films with very low damping obtained by recrystallization of amorphous material, *Scientific Reports* **6**, 20827 (2016).

[4] A. A. Serga, A. V. Chumak, and B. Hillebrands, Yig magnonics, *Journal of Physics D: Applied Physics* **43**, 264002 (2010).

[5] H. Yu, O. d'Allivy Kelly, V. Cros, R. Bernard, P. Bortolotti, A. Anane, F. Brandl, R. Huber, I. Stasinopoulos, and D. Grundler, Magnetic thin-film insulator with ultra-low spin wave damping for coherent nanomagnonics, *Scientific Reports* **4**, 6848 (2014).

[6] M. Collet, O. Gladil, M. Evelt, V. Bessonov, L. Soumah, P. Bortolotti, S. O. Demokritov, Y. Henry, V. Cros, M. Bailleul, V. E. Demidov, and A. Anane, Spin-wave propagation in ultra-thin YIG based waveguides, *Applied Physics Letters* **110**, 092408 (2017), https://pubs.aip.org/aip/apl/article-pdf/doi/10.1063/1.4976708/14495155/092408_1_online.pdf.

[7] Y. Li, T.-H. Lo, J. Lim, J. E. Pearson, R. Divan, W. Zhang, U. Welp, W.-K. Kwok, A. Hoffmann, and V. Novosad, Unidirectional microwave transduction with chirality selected short-wavelength magnon excitations, *Applied Physics Letters* **123**, 022406 (2023), https://pubs.aip.org/aip/apl/article-pdf/doi/10.1063/5.0156369/18038918/022406_1.5.0156369.pdf.

[8] L. J. Cornelissen, J. Liu, R. A. Duine, J. B. Youssef, and B. J. van Wees, Long-distance transport of magnon spin information in a magnetic insulator at room temperature, *Nature Physics* **11**, 1022 (2015).

[9] H. Huebl, C. W. Zollitsch, J. Lotze, F. Hocke, M. Greifenstein, A. Marx, R. Gross, and S. T. B. Goennenwein, High cooperativity in coupled microwave resonator ferromagnetic insulator hybrids, *Phys. Rev. Lett.* **111**, 127003 (2013).

[10] Y. Tabuchi, S. Ishino, T. Ishikawa, R. Yamazaki, K. Usami, and Y. Nakamura, Hybridizing ferromagnetic magnons and microwave photons in the quantum limit, *Phys. Rev. Lett.* **113**, 083603 (2014).

[11] X. Zhang, C.-L. Zou, L. Jiang, and H. X. Tang, Strongly

coupled magnons and cavity microwave photons, *Phys. Rev. Lett.* **113**, 156401 (2014).

[12] L. Bai, M. Harder, Y. P. Chen, X. Fan, J. Q. Xiao, and C.-M. Hu, Spin pumping in electrodynamically coupled magnon-photon systems, *Phys. Rev. Lett.* **114**, 227201 (2015).

[13] D. Lachance-Quirion, S. P. Wolski, Y. Tabuchi, S. Kono, K. Usami, and Y. Nakamura, Entanglement-based single-shot detection of a single magnon with a superconducting qubit, *Science* **367**, 425 (2020), <https://www.science.org/doi/pdf/10.1126/science.aaz9236>.

[14] D. Xu, X.-K. Gu, H.-K. Li, Y.-C. Weng, Y.-P. Wang, J. Li, H. Wang, S.-Y. Zhu, and J. Q. You, Quantum control of a single magnon in a macroscopic spin system, *Phys. Rev. Lett.* **130**, 193603 (2023).

[15] M. Haertinger, C. H. Back, J. Lotze, M. Weiler, S. Geprägs, H. Huebl, S. T. B. Goennenwein, and G. Woltersdorf, Spin pumping in yig/pt bilayers as a function of layer thickness, *Phys. Rev. B* **92**, 054437 (2015).

[16] H. Nakayama, M. Althammer, Y.-T. Chen, K. Uchida, Y. Kajiwara, D. Kikuchi, T. Ohtani, S. Geprägs, M. Opel, S. Takahashi, R. Gross, G. E. W. Bauer, S. T. B. Goennenwein, and E. Saitoh, Spin hall magnetoresistance induced by a nonequilibrium proximity effect, *Phys. Rev. Lett.* **110**, 206601 (2013).

[17] S. Klingler, V. Amin, S. Geprägs, K. Ganzhorn, H. Maier-Flaig, M. Althammer, H. Huebl, R. Gross, R. D. McMichael, M. D. Stiles, S. T. B. Goennenwein, and M. Weiler, Spin-torque excitation of perpendicular standing spin waves in coupled YIG/Co heterostructures, *Phys. Rev. Lett.* **120**, 127201 (2018).

[18] J. Chen, C. Liu, T. Liu, Y. Xiao, K. Xia, G. E. W. Bauer, M. Wu, and H. Yu, Strong interlayer magnon-magnon coupling in magnetic metal-insulator hybrid nanostructures, *Phys. Rev. Lett.* **120**, 217202 (2018).

[19] L. J. Cornelissen, J. Liu, R. A. Duine, J. B. Youssef, and B. J. van Wees, Long-distance transport of magnon spin information in a magnetic insulator at room temperature, *Nature Physics* **11**, 1022 (2015).

[20] Y. Li, W. Cao, V. P. Amin, Z. Zhang, J. Gibbons, J. Sklenar, J. Pearson, P. M. Haney, M. D. Stiles, W. E. Bailey, V. Novosad, A. Hoffmann, and W. Zhang, Coherent spin pumping in a strongly coupled magnon-magnon hybrid system, *Phys. Rev. Lett.* **124**, 117202 (2020).

[21] Y. Xiong, J. Inman, Z. Li, K. Xie, R. Bidhanapally, J. Sklenar, P. Li, S. Louis, V. Tyberkevych, H. Qu, Z. Xiao, W. K. Kwok, V. Novosad, Y. Li, F. Ma, and W. Zhang, Tunable magnetically induced transparency spectra in magnon-magnon coupled $y_3fe_5o_{12}$ /permalloy bilayers, *Phys. Rev. Appl.* **17**, 044010 (2022).

[22] J. Inman, Y. Xiong, R. Bidhanapally, S. Louis, V. Tyberkevych, H. Qu, J. Sklenar, V. Novosad, Y. Li, X. Zhang, and W. Zhang, Hybrid magnonics for short-wavelength spin waves facilitated by a magnetic heterostructure, *Phys. Rev. Appl.* **17**, 044034 (2022).

[23] Y. Fan, P. Quarterman, J. Finley, J. Han, P. Zhang, J. T. Hou, M. D. Stiles, A. J. Grutter, and L. Liu, Manipulation of coupling and magnon transport in magnetic metal-insulator hybrid structures, *Phys. Rev. Appl.* **13**, 061002 (2020).

[24] P. Quarterman, Y. Fan, Z. Chen, C. J. Jensen, R. V. Chopdekar, D. A. Gilbert, M. E. Holtz, M. D. Stiles, J. A. Borchers, K. Liu, L. Liu, and A. J. Grutter, Probing antiferromagnetic coupling in magnetic insulator/metal heterostructures, *Phys. Rev. Mater.* **6**, 094418 (2022).

[25] S. Klingler, V. Amin, S. Geprägs, K. Ganzhorn, H. Maier-Flaig, M. Althammer, H. Huebl, R. Gross, R. D. McMichael, M. D. Stiles, S. T. B. Goennenwein, and M. Weiler, Spin-torque excitation of perpendicular standing spin waves in coupled YIG/Co heterostructures, *Phys. Rev. Lett.* **120**, 127201 (2018).

[26] A. B. Shah, Q. M. Ramasse, J. G. Wen, A. Bhattacharya, and J. M. Zuo, Practical spatial resolution of electron energy loss spectroscopy in aberration corrected scanning transmission electron microscopy, *Micron* **42**, 539 (2011).